

# Radar-based Automotive Localization using Landmarks in a Multimodal Sensor Graph-based Approach

Stefan Jürgens  
MAN Truck & Bus SE  
stefan.juergens@man.eu

Niklas Koch  
Volkswagen AG  
niklas.koch@volkswagen.de

Marc-Michael Meinecke  
Volkswagen AG  
marc-michael.meinecke@volkswagen.de

**Abstract**—Highly automated driving functions currently often rely on a-priori knowledge from maps for planning and prediction in complex scenarios like cities. This makes map-relative localization an essential skill.

In this paper, we address the problem of localization with automotive-grade radars, using a real-time graph-based SLAM approach. The system uses landmarks and odometry information as an abstraction layer. This way, besides radars, all kind of different sensor modalities including cameras and lidars can contribute. A single, semantic landmark map is used and maintained for all sensors.

We implemented our approach using C++ and thoroughly tested it on data obtained with our test vehicles, comprising cars and trucks. Test scenarios include inner cities and industrial areas like container terminals. The experiments presented in this paper suggest that the approach is able to provide a precise and stable pose in structured environments, using radar data alone. The fusion of additional sensor information from cameras or lidars further boost performance, providing reliable semantic information needed for automated mapping.

## I. INTRODUCTION

Automated driving functions are a current focus of automotive research activities. These modern systems require rich and redundant sensor information. Additionally, a-priori knowledge, taken from maps, is needed for planning and prediction in complex scenarios like inner cities or container terminals. This makes a precise, map-relative localization an essential prerequisite for L4 and L5 driving functions in such complex environments.

Localization systems based on laser measurements, camera images and odometry information are well-known since decades. In contrast to this, radar-based odometry and localization are rather new techniques, under consideration of the research community since just a short time. While automotive-grade radars still suffer from a poor resolution compared to lidars, they provide undeniable advantages: reliable in harsh (weather-)conditions, tested and approved in the automotive mass market context for years, and thus quite cost-effective. In order to bring highly automated driving functions into series productions, these properties should be combined with the advantages of lidars and cameras to form a truly safe and redundant system.

In this paper, we deal with the integration of radars into a graph-based SLAM (Simultaneous Localization and Mapping) system [6]. Landmarks and odometry information are used as an abstraction layer, such that different types of sensors like radars, lidars, cameras and IMUs (inertial measurement units)

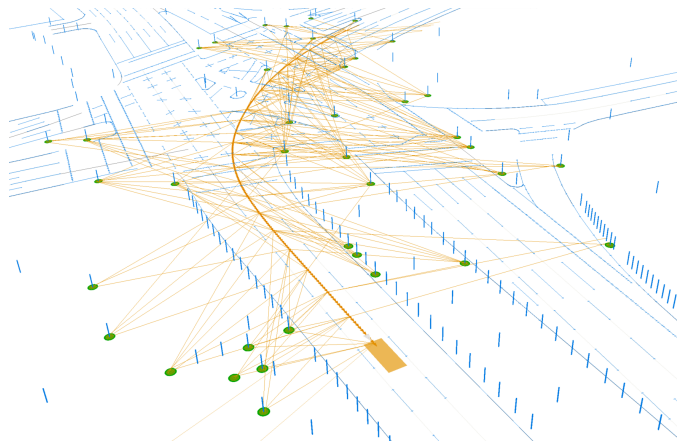


Fig. 1. SLAM graph of Hamburg inner city, run on radar data alone. Map in blue, landmark measurements in orange, map associations in green and localization pose in orange.

can contribute to a single, joint minimization problem. This also offers the possibility for a single semantic landmark map for all sensors, making maintaining such a map in a large scale, series scenario feasible. We use a third-party, pre-recorded map, which we partly enriched using our SLAM system.

The main contribution of this paper is a graph-based SLAM system, that can run both on radar data alone as well as on a wide, multimodal range of sensors. See Fig. 1 for an example. We achieve this by the extraction of landmarks and odometry information out of the untracked radar reflection points of a single measurement cycle in real-time. This allows us to provide a safe, redundant localization solution in real-world scenarios including inner cities and industrial areas like a container terminal.

In sum, we make these key claims: Our real-time SLAM approach is able to

- (i) localize with **automotive-grade radar data alone** in challenging scenarios like inner city and container terminals.
- (ii) fuse information of **different sensor modalities**: radar, lidar, camera, vehicle odometry and GNSS, using a **single, semantic landmark map** for all sensors.

These claims are backed up by the paper and our experimental evaluation in Sec. IV.

## II. RELATED WORK

There is already some literature on radar-based localization and its sub-problems. We present a short summary, divided into two main areas:

### A. Radar-based odometry

The radars on a vehicle measure the radial, relative velocity of the surrounding targets via the Doppler effect. Assuming that a good part of the environment is static, one can calculate the movement of the vehicle out of the Doppler velocities of these static targets. This is done in Kellner *et al.* [9], [8], putting all measurements in a large set of equations and solving them using different Least-Squares estimators (LSQ). Our own radar-based odometry follows this approach very closely, with a few additions.

Barjenbruch *et al.* [2] use a different, density-based framework. Here, measurements of Doppler radar sensors are represented as a mixture of Gaussian distributions. The ego-motion of the vehicle is obtained by calculating the transformation between these Gaussians of subsequent measurements. Both Doppler velocity and spatial information is used here. A variant with significant lower computational cost is presented in Rapp *et al.* [11]. As we want the spatial tracking to be solely on the landmark level, we do not follow this approach.

### B. Localization and Mapping

Ward and Folkesson [14] consider localization wrt. to a pre-recorded map. Two short range radars (SRR) provide point detections, which are registered to a map in every time step using the Iterative Closest Point algorithm (ICP). An Extended Kalman Filter (EKF) provides the map-relative vehicle pose.

Hammarsten and Runemalm [7] consider radars which provide measurements in both azimuth and elevation. They are used to construct 3D occupancy grid maps. Together with inertial measurements from the vehicle, they calculate a full 6D pose using two different methods: a particle filter and a registration-based algorithm.

In [10], Lupfer *et al.* show that the FastSLAM 2.0 algorithm benefits from the inclusion of radar data. They extend the measurement model for the landmarks to include, besides the usual angle and distance, also the Doppler information. Additionally to the radar landmarks, the vehicle odometry is used in the algorithm.

The approach by Schuster *et al.* [12] describes a complete, graph-based SLAM framework using 4 radars mounted on a car, providing 360° coverage. Point landmarks with unique descriptors are extracted from the data, associated to a map, and solved, together with an odometry from an IMU and wheel encoders, in a graph. This has similarities to our approach, but uses a wheel-based odometry and point landmarks that are specific for radars and do not necessarily correspond to semantic objects.

## III. OUR APPROACH

In this paper, we present a graph-based SLAM framework using landmark, odometry and global information. It has the following design goals:

- Fusion of information of **different sensor modalities**: radar, lidar, camera, odometry e.g. from inertial sensors and wheel encoders, and GNSS.
- Use of a **single, semantic landmark map** for all sensor modalities. It can be constructed by our system or pre-recorded by an external supplier.
- **Modularity**: Split of the system into the three parts: landmark extraction, odometry calculation and graph construction and minimization.
- **Sensor redundancy**: The system should perform stably with only a subset of possible sensor inputs, e.g. radar-only or lidar and odometry information alone.

The used graph-based approach was already presented in [16], [17], mainly run on lidar, odometry and GNSS data. We recap it shortly in Sec. III-A. The new feature presented in this paper is that we can run the SLAM algorithm on radar data alone. The calculation of the needed radar-based odometry is detailed in Sec. III-B, the landmark extraction is presented in Sec. III-C.

### A. Graph-based SLAM

In our landmark-based SLAM, we want to calculate the poses of the vehicle and landmarks that best fit to both the sensor measurements made in the past as well as to a pre-recorded map, if already existing. Measurements can be of the three types: landmark position, odometry measurement or global pose measurement (e.g. GNSS).

Writing this as a minimization problem, we define the state  $\mathbf{x} = [\mathbf{x}^p \ \mathbf{x}^l]$ , with the vehicle poses  $\mathbf{x}^p = [\mathbf{x}_1^p, \dots, \mathbf{x}_P^p]$  and landmark positions  $\mathbf{x}^l = [\mathbf{x}_1^l, \dots, \mathbf{x}_L^l]$ . The number of poses  $P$  determines the length of our sliding window, and  $L$  is the number of landmark estimates. Then the task is to solve

$$\mathbf{x}^* = \underset{\mathbf{x}}{\operatorname{argmin}} \sum_i e_i(\mathbf{x}, \mathbf{z}_i)^T \boldsymbol{\Omega}_i e_i(\mathbf{x}, \mathbf{z}_i) + \mathcal{F}^{map}(\mathbf{x}^l). \quad (1)$$

Here, we introduce the error functions  $e_i$  and the information matrices  $\boldsymbol{\Omega}_i$  related to the measurements  $\mathbf{z}_i$ . Both incorporate the information of the measurements and made associations with the map. They differ for the different measurement types of odometry, global poses, landmark observations and landmark map associations. For the latter, we can specify

$$\mathcal{F}^{map}(\mathbf{x}^l) = \sum_i e_i^{map}(\mathbf{x}^l)^T \boldsymbol{\Omega}_i^{map} e_i^{map}(\mathbf{x}^l) \quad (2)$$

with the error function  $e_i^{map}(\mathbf{x}^l) = \mathbf{x}_i^l - \mathbf{m}_i$ . The global positions of the map landmarks are given by  $\mathbf{m}_i$ .

This minimization problem can also be viewed as a factor graph: here, the state variables correspond to nodes, while measurements, error functions and information matrices can be seen as factors.

Our algorithm has three main steps. First in **local association**, new landmark measurements are associated to landmark states. These can be added to the graph. In the second step **map association**, landmark states are associated to the landmarks of the map. In the last **optimization** step, the problem is solved numerically. The library g2o [6] is used here.

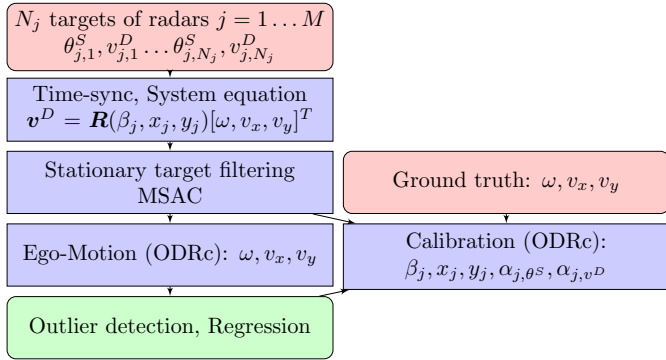


Fig. 2. The main steps of the radar-based odometry algorithm.

As landmarks, we use static, semantic objects that can be detected by different sensor modalities like radar, lidar and camera. This enables us to use a single, globally referenced landmark map for all sensors. Additionally, the landmark density should be sufficiently high in all considered scenarios. Examples are pole-like objects, building corners and planes, lane markings, curbs and guardrails.

For automotive-grade radars, this can lead to problems. Due to the 2D nature of the point data and the low point density, the extraction of semantic information is very difficult. Effectively, one can only extract point-like and line-like features out of the radar data. Associating these to semantic landmarks is quite unreliable. Using unique descriptors as in [12] could help, but they would need to be stored in the landmark map as well. We decided for a simpler approach, where we associate radar point features with poles, and radar line features with planes, curbs and guardrails. While for mapping this is quite problematic, for localization it works surprisingly well.

### B. Radar-based odometry

For the calculation of the odometry from the radar data, we closely follow the approach by Kellner *et al.* [9], [8]. Here, we present a short summary, including some tweaks and additions we made. For details, we refer to the original publications.

The basic idea of the approach is to use the measured Doppler velocity of the targets around the vehicle to obtain the ego-motion of the vehicle. This is possible as a large amount of targets is usually static, hence the Doppler velocities of these targets stem from the motion of the ego-vehicle. The algorithm flow is depicted in Fig. 2 and explained in the following.

In **Step 1**, the  $N_j$  untracked reflection points from different radars  $j = 1, \dots, M$  mounted on the vehicle are collected over a period of time, with Doppler velocity  $v_{j,i}^D$ , azimuth angle  $\theta_{j,i}^S$ , timestamp  $T_j$  and  $i \in \{1, \dots, N_j\}$ . They are put into a single system of equations, relating them to the vehicle's yaw rate  $\omega$  and velocity  $v_x$  and  $v_y$ :

$$\begin{bmatrix} \alpha_{1,v^D} \mathbf{v}_1^D \\ \vdots \\ \alpha_{M,v^D} \mathbf{v}_M^D \end{bmatrix} = \begin{bmatrix} \mathbf{M}_1 \mathbf{S}_1 \\ \vdots \\ \mathbf{M}_M \mathbf{S}_M \end{bmatrix} \begin{bmatrix} \omega \\ v_x \\ v_y \end{bmatrix}. \quad (3)$$

with  $\mathbf{v}_j^D = [v_{j,1}^D, \dots, v_{j,N_j}^D]^T$ . The matrices

$$\mathbf{S}_j = \begin{bmatrix} -y_j & 1 & 0 \\ x_j & 0 & 1 \end{bmatrix} \quad (4)$$

$$\mathbf{M}_j = \begin{bmatrix} \cos(\theta_{j,1}) & \sin(\theta_{j,1}) \\ \vdots & \vdots \\ \cos(\theta_{j,N_j}) & \sin(\theta_{j,N_j}) \end{bmatrix} \quad (5)$$

with  $\theta_{j,i} = \beta_j + \alpha_{j,\theta^S} \theta_{j,i}^S$  contain the mounting angle  $\beta_j$  and position  $(x_j, y_j)$  of the radar sensors mounted on the vehicle.  $\alpha_{j,v^D}$  and  $\alpha_{j,\theta^S}$  are scaling factors for every sensor added by us in order to deal with bias errors in measured Doppler velocity and azimuth angle. They are determined by our calibration procedure.

As an addition, we consider the time-sync of the data. The point data from different radars was measured at different times  $T_j$ , thus one should synchronize them to a common timestamp  $T_{odo}$ . The latter is ideally the middle of the measurement window, minimizing bias. This is done by replacing in Eq. (3)  $\mathbf{v}_j^D \Rightarrow \mathbf{v}_j^D - \Delta \mathbf{v}_j$  and  $\mathbf{M}_j \Rightarrow \mathbf{M}_j^{T_{odo}}$  with

$$\Delta \mathbf{v}_j = \mathbf{M}_j \mathbf{S}_j \begin{bmatrix} \omega^{T_j} \\ \mathbf{v}^{T_j} \end{bmatrix} - \mathbf{M}_j^{T_{odo}} \mathbf{S}_j \begin{bmatrix} \omega^{T_{odo}} \\ \mathbf{v}^{T_{odo}} \end{bmatrix} \quad (6)$$

$$\mathbf{M}_j^{T_{odo}} = \begin{bmatrix} \cos(\theta_{j,1} + \Delta\psi_j) & \sin(\theta_{j,1} + \Delta\psi_j) \\ \vdots & \vdots \\ \cos(\theta_{j,N_j} + \Delta\psi_j) & \sin(\theta_{j,N_j} + \Delta\psi_j) \end{bmatrix} \quad (7)$$

$$\Delta\psi_j = \psi^{T_j} - \psi^{T_{odo}}. \quad (8)$$

The needed rates  $(\omega^\tau, \mathbf{v}^\tau)^T$  and vehicle headings  $\psi^\tau$  at different times  $\tau \in \{T_j, T_{odo}\}$  can be obtained by extrapolation of the results of the last cycles of the odometry calculation.

In **Step 2**, a two stage filtering is applied to remove all targets from the equation which stem from moving objects in the vicinity of the ego-vehicle. At first, all measured velocities are compared to the ego-motion results of the last cycles and unreasonable data is thrown out, based on a simple vehicle model. Afterwards, the random consensus method MSAC [13] is used to retain only the static targets, which are expected to form the majority of the targets in the system of equations. As we want to obtain the 3 DOFs  $\omega$ ,  $v_x$  and  $v_y$ , this corresponds to fitting the data to a 3-dimensional plain. As  $v_y$  is usually small in most scenarios, we prefer for simplicity and lower run-time to subtract  $v_y$  from the equations, based on previous ego-motion results of the algorithm, and use MSAC together with a normal 2D plane. We choose the threshold distance  $d_{MSAC}$  of the data points to the plane based on the standard deviations  $\sigma_{v^D}$  and  $\sigma_{\theta^S}$  of the measured variables  $v_{j,i}^D$  and  $\theta_{j,i}^S$ , which is provided by the radar manufacturer. Choosing  $d_{MSAC}$  such that between 60% and 80% of the static measurements are used leads to the best results for us.

In **Step 3a** we obtain the ego-motion solution for  $(\omega, v_x, v_y)^T$ , using the orthogonal distance regression algorithm with bias compensation (ODRc).

In **Step 4a**, the obtained ego-motion is compared to the previous results to detect outliers. In these failure cases, we perform a regression over the previous ego-motion results

to obtain a best guess for the vehicle state at the present timestamp.

The ego-motion result is very sensitive to deviations in the calibration of the yaw angle of the mounted sensors. We therefore implemented a second path (**Step 3b**) of the algorithm, used for calibration. Here, we take the ego-motion result  $(\omega, v_x, v_y)^T$ , either from a reference system or from the radar odometry itself, and calculate the calibration parameters  $(\beta_j, x_j, y_j, \alpha_{j,vD}, \alpha_{j,\theta S})^T$  for every radar separately. In the online configuration, the parameters are calculated every cycle and collected in a median filter to obtain the most likely calibration parameters after a longer period of time, e.g. a drive of 10 min. In the offline version, the measurements of the complete drive, minus outliers, are collected and optimized as a whole. This leads to better calibration parameters, especially for the sensor mounting positions which can only be reliably determined in driving situations with a finite yaw rate.

The algorithm works very precisely and reliably, if enough static targets are available. A  $360^\circ$  coverage of the surroundings of the vehicle is thus recommended. This way, the algorithm remains stable also in difficult situations like dense traffic, as shown in Sec. IV-D.

### C. Radar feature detection

Besides the odometry information, the graph needs landmark measurements to estimate a map relative pose. The main problem here is that our radar data is noisy and only 2D, see Sec. IV-A. This makes it hard to extract semantic information about the measured objects, which would be necessary to distinguish landmarks of specific type. We therefore restrict ourselves to extract point-like and line-like features out of the measured radar data. These are then associated to landmarks as described in Sec. III-A.

**Step 1:** The untracked reflection point data of all radars is aggregated for some time, in our case 400 ms. Using the Doppler velocity and odometry information, all points from moving objects are filtered out.

**Step 2:** We find point-like clusters in the data using the density-based clusterer OPTICS [1]. It is well-suited for the detection of clusters with different densities, which occur due to the different reflection point density of the radar data. All reflection points belonging to a point-like feature are removed from the data set.

**Step 3:** We search for line-like feature in the remaining set of points. MSAC [13] is used for this. Optionally, overlapping line segments can be merged.

## IV. EXPERIMENTAL EVALUATION

The experiments are designed to show the capabilities of our method and to support our key claims, that our real-time SLAM approach is able to (i) localize with **automotive-grade radar data alone** and (ii) fuse information of the **different sensor modalities** radar, lidar, camera, vehicle odometry and GNSS, using a **single, semantic landmark map** for all sensors.



Fig. 3. Sensor setup of our vehicles. The cars use the 6 radars on the corners and on the sides, the trucks currently only 4: the two on the sides and on the front corners, respectively.

All experiments are performed with our car or truck test vehicles presented in Sec. IV-A. The driven scenarios are presented in Sec. IV-B. The overall localization performance of the full system is evaluated in Sec. IV-C on this real world data against a reference system. In Sec. IV-D, we have a closer look at the stability and precision of the radar-based odometry, deducing necessary, scenario dependent criteria under which the performance of the odometry, and the whole localization system running on radar data alone, remains stable.

### A. Test Vehicles: Car and Truck

We perform our experiments on two different test vehicles: an e-Golf 7 and a MAN semi-trailer truck, see Fig. 3. While the vehicles look and drive quite differently, the sensor setup is similar. They use wheel encoders and an IMU for the classical vehicle odometry, a close-to-series GNSS receiver, Velodyne lidars, a front camera for lane detection, and have a reference-grade RTK system installed: for the truck it's an ADMA, for the car an Applanix. Both use 77 GHz automotive-grade radars: While the cars have a  $360^\circ$  coverage by 6 short range radars (SRR), the trucks only use 4 of the SRRs. An additional long range radar in the front is currently not used in our experiments. The radars are installed at a height of 40-70 cm which is not optimal for localization purposes as their line of sight to landmarks is often blocked by other traffic participants. The data rate is 20 Hz, which we also choose as the output frequency of the odometry.

Corominas-Murtra *et al.* [3] show that for odometry calculations, pairs of radars mounted diagonally on the vehicle perform best. Therefore we expect the truck setup to be less optimal than the car setup. In general, our current automotive-grade radars provide only 2D point clouds and suffer from poor resolution. New developments like synthetic aperture radars (SARs) discussed by Gisder *et al.* [4], [5] or polarimetric radars presented in [15] are expected to improve the data quality significantly in the future.

### B. Test Scenarios: Inner City and Container Terminal

Our test scenarios cover two of the relevant and complex cases for cars and trucks: **Hamburg inner city** and a **container terminal** in Hamburg harbor. During the drive, traffic was quite dense (moderate) in the city (terminal), respectively. Third-party, pre-recorded maps based on high dense lidar data, that were initially meant for lidar and camera-based localization, not radars, are used here. This works fine,

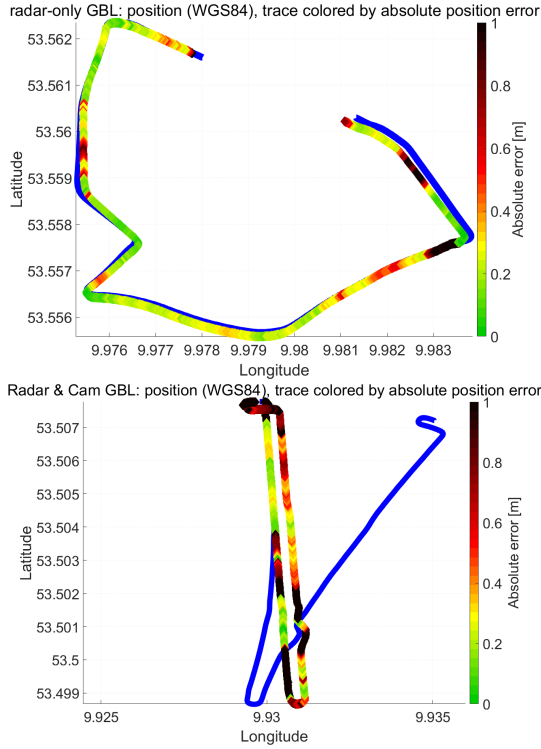


Fig. 4. Driven paths for the city (top) and terminal (bottom) scenario. The colors indicate the absolute position error of the radar-only (top) and radar & camera (bottom) graph-based localization (GBL) wrt. the reference system. Additionally, the path of the radar odometry is plotted in blue.

TABLE I  
STANDARD DEVIATION OF THE LATERAL AND ABSOLUTE POSITION ERROR WRT. THE REFERENCE. FOR  $1\sigma$  ( $2\sigma$ ), 68.2% (95.4%) OF THE ERRORS ARE BELOW THE GIVEN VALUE.

	$1\sigma$ city	$2\sigma$ city	$1\sigma$ termi.	$2\sigma$ termi.
radar-only lat.	0.25 m	1.07 m	0.75 m	>2 m
radar-only abs.	0.32 m	1.41 m	1.16 m	>2 m
radar & camera lat.	0.13 m	0.76 m	0.27 m	1.79 m
radar & camera abs.	0.20 m	>2 m	0.98 m	>2 m
full setup lat.	0.07 m	0.18 m	0.17 m	0.28 m
full setup abs.	0.15 m	0.28 m	0.24 m	0.45 m

although the radar sees the world a bit differently compared to a lidar, e.g. detecting the poles of a guardrail instead of the rail itself.

In the experiments, we compare the driven paths for radar odometry and the localization system in the three cases radar-only, radar & camera localization, and the full sensor setup including the lidars and the vehicle odometry. The RTK reference systems of the vehicles serve as ground truth. The driven paths are visualized in Fig. 4, where the color coding indicates the absolute position error. The paths obtained by the radar odometry alone are shown in blue.

### C. Overall Localization Accuracy

The standard deviation of the lateral and absolute position error wrt. the reference is shown in Tab. I. Plots of the cumulative distribution function (CDF) for the radar-only and radar & camera case are presented in Fig. 5.

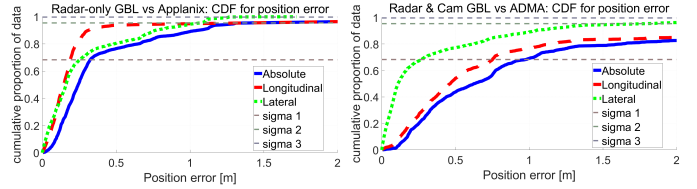


Fig. 5. The CDF plots of the radar-only graph-based localization (GBL) for the city (left) and the radar & camera localization for the terminal (right) scenario.

*Radar only:* In the city scenario, radar alone performs very well due to the abundance of static infrastructure. This leads to an accurate radar-based odometry and good landmark detections. Inaccuracies arise if the line of sight to the landmark is blocked by other static objects like parking cars. This can lead to wrong map association, which happened in the two areas in Fig. 4 (up) with the error being larger than 1 m.

The terminal is more difficult. The odometry suffers from a drift in some areas, which will be discussed in Sec. IV-D in more details. Additionally, parked containers block the line of sight to the mapped static infrastructure, and are regularly mistaken for buildings. In these cases, the localization accuracy deteriorates to the level of the GNSS receiver or even below. Therefore, the 4 radars of our sensor setup alone are not enough for a stable localization in this scenario.

*Radar and camera:* The lane markings from the front camera increase the accuracy and stability of our localization approach. The latter stems from the higher landmark density and variety, such that wrong map association can be avoided. Yet, lane markings usually do not compensate longitudinal errors and can introduce additional errors and noise in complex areas like crossings.

*Lidar, radar, camera and vehicle odometry:* Including the full sensor setup, our approach performs at least as good as post-processed RTK systems in the discussed scenarios, especially in the city. The determined  $1\sigma$  ( $2\sigma$ ) distances in the lower rows of Tab. I give therefore the boundaries of the accuracy of our reference systems. The worse numbers for the terminal stem from the fact that we only post-processed the Applanix, but used the online pose of the ADMA.

### D. Radar Odometry Accuracy and Robustness

Aside from the landmark detections, the localization performance depends on the stability and accuracy of the used odometry. For our radar-based odometry, we identified two main problems occurring in our scenarios.

**Drift due to vacancy:** In the case that there is an abundance of static environment on one side of the ego-vehicle and nothing on the other (or a moving object is filtered out there), the odometry tends to calculate a false yaw rate leading to a small drift to the free side. A possible reason might be small calibration errors which usually cancel each other out if all radars contribute equally to the odometry. Yet, as all radars are calibrated independently of each other, such an interdependency between them should not occur. Adding the

## V. CONCLUSION

In this paper, we presented a novel approach to use automotive-grade radar data for localization. Our method exploits a graph-based formulation using landmarks and odometry information, enabling a fusion of different sensor modalities while maintaining only a single, semantic landmark map. This allows us to successfully localize with radar data alone, as well as with an arbitrary combination of radar, lidar, and camera information.

We implemented and evaluated our approach on different datasets taken with car and truck test vehicles. Our experiments suggest that radar-only localization works precisely and reliably in many scenarios, e.g. in inner cities. A fusion with additional sensor modalities like cameras and lidars can provide more detailed, semantic information, especially useful for mapping.

## REFERENCES

- [1] M. Ankerst, M.M. Breunig, H.-P. Kriegel, and J. Sander. Optics: Ordering points to identify the clustering structure. pages 49–60. ACM Press, 1999.
- [2] M. Barjenbruch, D. Kellner, J. Klappstein, J. Dickmann, and K. Dietmayer. Joint Spatial- and Doppler-based Ego-Motion Estimation for Automotive Radars. In *Proc. of the IEEE Intel. Veh. Symp. (IV)*, 2015.
- [3] A. Corominas-Murtra, J. Vallvé, J. Solà, I. Flores, and J. Andrade-Cetto. Observability Analysis and Optimal Sensor Placement in Stereo Radar Odometry. In *Proc. of the IEEE Intl. Conf. on Rob. & Auto. (ICRA)*, 2016.
- [4] T. Gisder, F. Harrer, and E. Biebl. Application of a stream-based sar-backprojection approach for automotive environment perception. In *International Radar Symposium (IRS)*, 2018.
- [5] T. Gisder, M.-M. Meinecke, and E. Biebl. Synthetic aperture radar towards automotive applications. In *International Radar Symposium (IRS)*, 2019.
- [6] G. Grisetti, M. Barjenbruch, C. Stachniss, and W. Burgard. A tutorial on graph-based SLAM. *IEEE Trans. on Intel. Tra. Sys. Mag.*, 2:31f, 2010.
- [7] M. Hammarsten and V. Runemalm. 3d localization and mapping using automotive radar. Master's thesis, Chalmers University of Technology, Department of Signals and systems, 2016.
- [8] D. Kellner. *Verfahren zur Bestimmung von Objekt- und Eigenbewegung auf Basis der Dopplerinformation hochauflösender Radarsensoren*. PhD thesis, Universität Ulm, 2016.
- [9] D. Kellner, M. Barjenbruch, J. Klappstein, J. Dickmann, and K. Dietmayer. Instantaneous Ego-Motion Estimation using Multiple Doppler Radars. In *Proc. of the IEEE Intl. Conf. on Rob. & Auto. (ICRA)*, 2014.
- [10] S. Lupfer, M. Rapp, K. Dietmayer, P. Brosseit, J. Lombacher, M. Hahn, and J. Dickmann. Increasing FastSLAM Accuracy for Radar Data by Integrating the Doppler Information. In *Proc. of the IEEE Intl. Conf. on Microwaves for Intelligent Mobility (ICMIM)*, 2017.
- [11] M. Rapp, M. Barjenbruch, K. Dietmayer, M. Hahn, and J. Dickmann. A Fast Probabilistic Ego-Motion Estimation Framework for Radar. In *Proc. of the Europ. Conf. on Mobile Robotics (ECMR)*, 2015.
- [12] F. Schuster, C.G. Keller, M. Rapp, M. Haeuis, and C. Curio. Landmark based Radar SLAM Using Graph Optimization. In *Proc. of the IEEE Intl. Conf. on Intelligent Transportation Systems (ITSC)*, 2016.
- [13] P.H.S. Torr and A. Zisserman. MLESAC: A new robust estimator with application to estimating image geometry. *Computer Vision and Image Understanding*, 78:138–156, 2000.
- [14] E. Ward and J. Folkesson. Vehicle localization with low cost radar sensors. In *Proc. of the IEEE Intel. Veh. Symp. (IV)*, 2016.
- [15] F. Weishaupt, K. Werber, J. Tilly, J. Dickmann, and D. Heberling. Polarimetric Radar for Automotive Self-Localization. In *International Radar Symposium (IRS)*, 2019.
- [16] D. Wilbers, C. Merfels, and C. Stachniss. Localization with sliding window factor graphs on third-party maps for automated driving. In *Proc. of the IEEE Intl. Conf. on Rob. & Auto. (ICRA)*, 2019.
- [17] D. Wilbers, L. Rumberg, and C. Stachniss. Approximating marginalization with sparse global priors for sliding window SLAM-graphs. In *Proc. IEEE Int. Conf. Robotic Computing*, 2019.

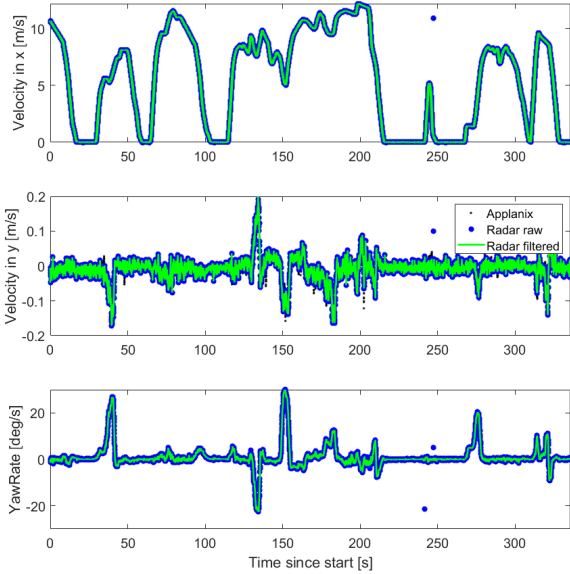


Fig. 6. Yaw rate and velocities of the radar odometry for the Hamburg city scenario. Radar raw (filtered) is the signal without (with) outlier rejection, respectively.

scaling factors  $\alpha_{j,vD}$  and  $\alpha_{j,\theta S}$  (see Sec. III-B) reduced the problem significantly. Still, the sensor model is quite basic and should be extended.

**Drift / breakdown due to moving objects:** Dense traffic can lead to inaccuracies, if it is not filtered out completely. This occurs especially in stop-and-go situations with low ego-velocity. For the Hamburg city scenario this is only a minor problem, as indicated by the good odometry path in Fig. 4 (up). Additionally, we plot the velocities and yaw rate of the radar odometry in Fig. 6. During the whole drive the algorithm provided a stable solution, with the outlier detection and regression step being triggered only in two cycles (blue outliers in Fig. 6). The residuals have mean and standard deviation of

$$r_{vx} = 0.0046 \pm 0.019 \frac{\text{m}}{\text{s}} \quad (9)$$

$$r_{vy} = -0.0011 \pm 0.014 \frac{\text{m}}{\text{s}} \quad (10)$$

$$r_{yawrate} = -0.0052 \pm 0.40 \frac{\text{deg}}{\text{s}}. \quad (11)$$

Thus the algorithms works very precisely and stably in dense traffic, which we attribute to the  $360^\circ$  coverage of the radars.

For the truck in the terminal, two situations of breakdown occurred at the beginning and end of the drive: in both cases, a tractor-trailer crosses directly in front of our own truck, such that the majority of radar reflection points no longer stem from the static environment. As this crossing takes several seconds, the outlier detection and regression step can only partly cope with the problem. Additional radars that look at the back of the truck or are installed on the semi-trailer will easily fix this problem.